HHS Public Access

Author manuscript

J Am Chem Soc. Author manuscript; available in PMC 2024 January 15.

Published in final edited form as:

J Am Chem Soc. 2023 December 20; 145(50): 27336–27347. doi:10.1021/jacs.3c07491.

CytoDirect: A Nucleic Acid Nanodevice for Specific and Efficient Delivery of Functional Payloads to the Cytoplasm

Lu Yu,
School of Molecular Sciences and Center for Molecular Design and Biomimetics, The Biodesign Institute, Arizona State University, Tempe, Arizona 85281, United States

Yang Xu,
School of Molecular Sciences and Center for Molecular Design and Biomimetics, The Biodesign Institute, Arizona State University, Tempe, Arizona 85281, United States

Md Al-Amin,
School of Molecular Sciences and Center for Molecular Design and Biomimetics, The Biodesign Institute, Arizona State University, Tempe, Arizona 85281, United States

Shuoxing Jiang,
School of Molecular Sciences and Center for Molecular Design and Biomimetics, The Biodesign Institute, Arizona State University, Tempe, Arizona 85281, United States

Matthew Sample,
School of Molecular Sciences and Center for Molecular Design and Biomimetics, The Biodesign Institute, Arizona State University, Tempe, Arizona 85281, United States

Abhay Prasad,
School of Molecular Sciences and Center for Molecular Design and Biomimetics, The Biodesign Institute, Arizona State University, Tempe, Arizona 85281, United States

Nicholas Stephanopoulos,
School of Molecular Sciences and Center for Molecular Design and Biomimetics, The Biodesign Institute, Arizona State University, Tempe, Arizona 85281, United States

Petr Šulc,
School of Molecular Sciences and Center for Molecular Design and Biomimetics, The Biodesign Institute, Arizona State University, Tempe, Arizona 85281, United States

Hao Yan

Corresponding Author: **Hao Yan** – *School of Molecular Sciences and Center for Molecular Design and Biomimetics, The Biodesign Institute, Arizona State University, Tempe, Arizona 85281, United States*; hao.yan@asu.edu.

Author Contributions

The manuscript was written through contributions of all authors. All authors have given approval to the final version of the manuscript.

Notes Competing interests: L.Y., Y.X., M.A., S.J., N.S., and H.Y. filed US patents covering aspects of this work.

Supporting Information

The Supporting Information is available free of charge at https://pubs.acs.org/doi/10.1021/jacs.3c07491.

Multiple Supporting Figures and nucleic acid/protein sequences (Figures S1–S36) (PDF)

Complete contact information is available at: https://pubs.acs.org/10.1021/jacs.3c07491

The authors declare the following competing financial interest(s): The authors have filed patents covering aspects of this work.

School of Molecular Sciences and Center for Molecular Design and Biomimetics, The Biodesign Institute, Arizona State University, Tempe, Arizona 85281, United States

Abstract

Direct and efficient delivery of functional payloads such as chemotherapy drugs, siRNA, or small-molecule inhibitors into the cytoplasm, bypassing the endo/lysosomal trapping, is a challenging task for intracellular medicine. Here, we take advantage of the programmability of DNA nanotechnology to develop a DNA nanodevice called CytoDirect, which incorporates disulfide units and human epidermal growth factor receptor 2 (HER2) affibodies into a DNA origami nanostructure, enabling rapid cytosolic uptake into targeted cancer cells and deep tissue penetration. We further demonstrated that therapeutic oligonucleotides and small-molecule chemotherapy drugs can be easily delivered by CytoDirect and showed notable effects on gene knockdown and cell apoptosis, respectively. This study demonstrates the synergistic effect of disulfide and HER2 affibody modifications on the rapid cytosolic delivery of DNA origami and its payloads to targeted cells and deep tissues, thereby expanding the delivery capabilities of DNA nanostructures in a new direction for disease treatment.

Graphical Abstract

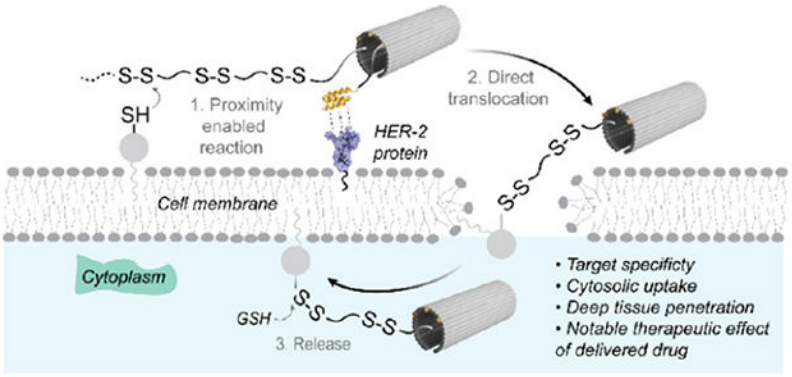

INTRODUCTION

Nanomedicine aims to utilize the chemical and physical properties of nanomaterials for the diagnosis and treatment of diseases at the molecular or nanoscale level.[1] However, the therapeutic potential of various drug modalities—including oligonucleotides like mRNAs and siRNA, proteins, plasmids, and antitumor drugs—has not been fully realized due to their poor cell membrane permeability, endo/lysosomal entrapment, enzymatic degradation, and rapid liver clearance.[2–6] Enhancing drug delivery to tumors and achieving efficient intracellular drug release are considered important goals in precision medicine. Different strategies have been employed to address these challenges, including using carriers like virus-like particles, organic nanoparticles (e.g., liposomes, synthetic polymers, and micelles), and inorganic nanoparticles (e.g., mesoporous silica nanoparticles and gold nanoparticles).[7–12] Nevertheless, the development of rapid and efficient cytosolic drug delivery nanomaterials with target specificity and biocompatibility remains a great challenge

in the field of nanomedicine. Further research is needed to address these challenges and optimize the use of nanomaterials in disease treatment.

Scaffolded DNA origami has emerged as a promising drug delivery platform, owing to its unique features such as the ability to generate complex prescribed shapes, with tunable size, surface functionalization, and biocompatibility.[13–16] A plethora of studies have explored the potential of using DNA origami as nanocarrier for therapeutic molecules.[17–19] However, a significant challenge faced by many nanocarriers (including DNA origami-based structures) is their susceptibility to entrapment within endosomes/lysosomes, which leads to subsequent degradation in the highly acidic and enzymatic environment of these organelles.[20] Therefore, the therapeutic efficacy of the loaded drugs that require cytosolic delivery or subcellular localization is heavily compromised.

The discovery of endocytosis-independent pathways, such as counterion-mediated uptake, membrane fusion, and thiol-mediated uptake, has paved the way for novel approaches to achieve direct cytosolic delivery of biomolecules.[21] In 2012, Gait and co-workers introduced the concept of thiol-mediated uptake, which employs dynamic covalent disulfide exchange chemistry with the aim of covalently attaching transporters to the cell surface, thus facilitating uptake.[22] Conjugation of cyclic or linear disulfide units to single-stranded oligonucleotides or short peptides has shown some initial evidence for cytosolic internalization,[23,24] but these systems lack cell targeting specificity, high cargo loading capacity, and the modularity required to engineer multifunctional nanocarriers.

The human epidermal growth factor receptor 2 (HER2) is overexpressed in some malignant cells, especially breast cancer cells. Therefore, HER2 is an attractive target for cancer diagnosis and therapy.[25] Anti-HER2 antibodies (Trastuzumab, Pertuzumab, and Ertumaxomab) have been widely used for cancer treatment.[26] However, their immunogenicity and difficulties in traversing the cell membrane have hampered their biomedical applications. The HER2 affibody is a small protein of 58 amino acids (~6KD) with high binding affinity to the HER2 protein [KD = 22pM].[27] It can be easily expressed in *Escherichia coli* and modified with other molecules for targeting purposes.[28,29]

Here, we developed a novel CytoDirect DNA nanodevice that integrates disulfide and HER2 affibody modifications on DNA origami, enabling fast cytosolic delivery of therapeutic drugs to target cancer cells and deep tissue (Figure 1a). The disulfide units facilitate the rapid internalization of the delivered drugs into the cytosol, while the HER2 affibody serves both as a targeting domain and as a regulator, bringing the disulfide units into close proximity to cell surface thiol groups in order to accelerate the rate of disulfide exchange, which is critical for membrane penetration. Upon cellular uptake, CytoDirect was rapidly released to the cytosol by endogenous glutathione (GSH) (Figure 1b). Notably, CytoDirect exhibited a uniform and diffuse distribution throughout the cytoplasm, thereby overcoming a common limitation observed in drug delivery vehicles, specifically the tendency to aggregate into large punctate spots within the cytoplasm. These aggregates can hinder the effective delivery of drugs to their intended targets. CytoDirect exhibits high cytosolic uptake solely in HER2 overexpressed cancer cells as well as excellent tumor penetration in deep tissue. Moreover, therapeutic oligonucleotides and small molecular anticancer drugs delivered by

CytoDirect demonstrated efficient gene knockdown and cell apoptosis effects, respectively. These results suggest that CytoDirect is a promising platform for cytosolic delivery in targeted cancer cells and deep tissue with potential applications in the treatment of various diseases.

RESULTS AND DISCUSSION

Design, Construction, and Characterization of CytoDirect.

To prepare CytoDirect (Figure 1a), a DNA origami nanosheet (DON) measuring approximately 90 nm × 60 nm × 2 nm—was synthesized using a 7249-nucleotide-long M13 bacteriophage genome DNA and hundreds of staple strands (Figures 1c and S1). To control the orientation of drug loading on the inner side of the nanosheet, an internal curvature was introduced to counteract the entropically unfavorable electrostatic repulsions generated by the large number of extended DNA overhangs.[30] The desired curvature was rationally designed by manipulating the spacing between the crossovers of the DNA nanostructure. To screen the design space of crossover spacings, simulations using the coarse-grained DNA model (oxDNA)[31] were performed to predict the structural curvature of the DON. The introduction of an increasing number of overhang extension cargo loading sites on the DON effectively neutralized the introduced curvature, until a total left-shift of 18 bases in vertical crossovers was implemented (Figures S2–S7). Consequently, all of the following experiments were carried out based on the 18-base left-shifted DNA nanostructure. Disulfide unit modification of DNA strands was achieved using phosphoramidite chemistry (Scheme S1 and Figures S8–S11). A linear *tert*-butyl disulfide with 6-repeats (6SS) was introduced at the 5′ end of single-stranded DNA following a previously reported protocol.[23] HPLC was used to purify FAM-labeled 6SS-DNA, which was then characterized by MALDI-TOF-MS (Figures S12–S14 and Table S1). There are two primary reasons for selecting FAM as the labeling dye for tracking the cellular uptake of disulfide-modified DNA origami. First, FAM is pH-sensitive compared with other commonly used dyes (Alexa Fluor 488 and Cy5 dyes), particularly within the range of 4.5–6.5, which corresponds to the acidic pH environment found in the late endosomes and lysosomes (Figure S15).[32] Therefore, we should not see an obvious fluorescent signal when DNA origami is trapped in the acidic organelles, which helps to better monitor the cytosolic uptake process. To determine how many structures were trapped in endosomes vs directly delivered to the cytoplasm, we also tested cellular uptake with the pH-insensitive fluorophore, Alexa Fluor 488 (Figure S32). Second, it has been reported that free Cy5 and Cy5 labeled DNA exhibited strong cell internalization within various mammalian cells, which might be attributed to the positive charge of the cyanine dyes and accumulation in mitochondria.[33,34] Therefore, labeling Cy5 for DNA nanostructure might not provide a distinct difference in the cellular uptake solely due to the specific modification.[35]

The HER2 affibody-DNA conjugate was synthesized by attaching amine-DNA to HER2 affibody molecules, which were expressed in *E. coli* cells, using the cross-linker sulfo-SMCC (sulfosuccinimidyl-4-[*N*-maleimidomethyl]-cyclohexane-1-carboxylate). The HER2 affibody-DNA conjugate was purified by FPLC and characterized by SDS-PAGE (Figure S16). The 6SS-DNA and HER2 affibody-DNA were loaded onto the DON through

hybridization with complementary ssDNA overhang extensions on the DON. After assembly, CytoDirect was characterized by using native agarose gel electrophoresis. Discrete bands with the expected mobility shift were observed for nanostructures without disulfide modification, suggesting the formation of designed nanostructures. However, 6SS-DNA-loaded DON moved faster than 0SS-DNA-loaded DON and exhibited a dimer band, signaling a morphological change (Figure S17). This result was further verified by transmission electron microscopy (TEM). Most DONs showed a rectangular morphology, while approximately 15% displayed a tubular structure. Interestingly, all DONs exhibited a tubular shape after disulfide modification, with around 30% forming a dimer, a result attributed to the hydrophobic effect introduced by the *tert*-butyl protecting groups on the disulfide patch of the DON (Figures 1c and S18–S22). This morphology can safeguard payloads within the tubular structure to a certain extent, and the hydrophobic effect can also enhance cellular uptake by increasing the interaction between the cell membrane and CytoDirect. Crucially, the designed curvature aided in preventing the formation of aggregates due to the hydrophobic *tert*-butyl interactions. We found that the tubular disulfide-modified DON unfolded in the presence of the surfactant Tween 80 from AFM images but not in the presence of GSH, suggesting the tubular conformation was induced by hydrophobic actuation instead of undesired thiol group cross-linking (Figure S23). Overall, these results demonstrated the successful self-assembly of CytoDirect.

In order to determine whether 0SS-DNA or 6SS-DNA conjugates can be quantitatively loaded onto the DON, we measured the fluorescence intensity of DNA origami (S24a). Different numbers of capture staple strands (0, 26, 51, 101, and 189) were incorporated during the synthesis of the DNA origami, which was subsequently loaded with the corresponding amount of FAM-labeled 0SS-DNA or 6SS-DNA. We labeled each DNA origami with four Alexa Fluor 647 fluorophores to normalize the fluorescence result. By comparing the relative fluorescence intensity of the samples with the expected fluorescence (of 100% incorporation), we were able to determine the amount of DNA loaded on the DON. The excitation wavelengths of FAM and Alexa Fluor 647 are 490 and 650 nm, respectively. As illustrated in Figure S24a, the DNA origami, regardless of disulfide modification, exhibited fluorescence intensity similar to the maximum expected value under varying DNA amounts. This indicated that the amount of 0SS-DNA or 6SS-DNA loaded on the DNA origami can be controlled quantitatively. We also evaluated the stability of the disulfide-modified DON by incubating it in a cell culture medium (with 10% FBS). Disulfide-modified DON remained largely intact for at least 24 h (Figure S24b,c). We assessed the cytotoxicity of the disulfide-modified DON using a cell counting kit-8 (CCK-8) assay (Figure S25), and it showed no cytotoxicity to HeLa cells, demonstrating its biocompatibility. By contrast, commercially available lipofectamine exhibited clear cytotoxicity to cells. The reason why 6 nM DNA origami showed some slight cytotoxicity to the cells might be because of the increased dilution of the cell complete medium, which changed the nutrient and osmotic pressure of the extracellular environment.

Target Specificity of CytoDirect to HER2 Overexpressed SK-BR-3 Breast Cancer Cells.

To investigate the selectivity of CytoDirect for specific cells, we analyzed breast cancer cell lines that express varying levels of HER2 protein (specifically, SK-BR-3 and MCF-7 cell

lines). We found that the expression of HER2 protein in SK-BR-3 cells was significantly higher (~20.4-fold) than in MCF-7 cells, as determined by flow cytometry (Figure S26). We conducted a qualitative assessment of the amount of HER2 affibody (0, 1, 3, and 5) on DON loaded with 0SS-DNA (0SS-DON) and DON loaded with 6SS-DNA (6SS-DON) using confocal laser scanning microscopy (CLSM). It was found that three HER2 affibodies on each DNA origami were potent enough for targeting HER2-overexpressing cells (Figure 2a). We then compared the targeting ability of CytoDirect (DSHAF-DON), HER2 affibody-modified DNA origami (HAF-DON), and disulfide-modified DNA origami (DS-DON) in SK-BR-3 and MCF-7 cells by CLSM (Figure 2b,c). We labeled the DON with Fluorescein (FAM) to track its location.

Confocal imaging revealed that both CytoDirect and HAF-DON could bind to the surface of SK-BR-3 cells but barely bind to MCF-7 cells. This indicates the selectivity of HER2 affibody-modified DON for HER2-overexpressing cells. However, without HER2 affibody modification, only negligible green fluorescence was observed, further confirming that target specificity was induced by the HER2 affibody. This result suggest that CytoDirect could be a potentially safer and more efficient drug carrier for cancer treatment.

CytoDirect Uptake Process by SK-BR-3 Cells.

Having validated the construction of CytoDirect and its selectivity for HER2-positive SK-BR-3 cells, we next demonstrated its cellular uptake efficiency both qualitatively and quantitatively using CLSM and flow cytometry. A time-course study (5 min, 30 min, 1 h, 3 h, 5 h, 7 h, 9 h, and 12 h) was conducted to examine the cellular uptake over time by CLSM (Figures 3a and S27).

In light of the fact that HAF-DON also rapidly bound to SK-BR-3 cells (Figure 2c), we used HAF-DON as a control to specifically assess the impact of disulfide modification and eliminate the interference of the HER2 affibody on cellular uptake. CytoDirect began binding to SK-BR-3 cells within 5 min. Extending the duration to 30 min, the accumulation of CytoDirect around the cell membrane initiated the translocation process. From approximately 3–7 h, most of CytoDirect was released from the internal cell membrane, as observed by the decreased fluorescence intensity on the cell membrane and the distribution of fluorescence throughout the cytosol, which persisted even after 12 h (Figure S27). It is noteworthy that the distribution of CytoDirect inside the cytoplasm was predominately homogeneous, with only very few bright punctate spots (which are distinctive features of late endo/lysosomal sequestration). By contrast, HAF-DONs were hardly taken up inside the SK-BR-3 cells but remained on the cell membrane, further confirming the significant influence of the disulfide modification on the cellular uptake. We next performed flow cytometry experiments to further confirm this selective uptake.

We compared the cellular uptake of DON, DS-DON, HAF-DON, and CytoDirect with FAM labels on the loaded 6SS- or 0SS-modified capture strands (Figure 3b). We observed a 5.3-fold increase in the uptake in SK-BR-3 cells for CytoDirect, compared to HAF-DON; an 11.3-fold increase for CytoDirect compared to DS-DON; and about a 55-fold increase for CytoDirect compared to DON. These results suggested that both the HER2 affibody and disulfide modification were critical to the cellular uptake. The combination of the HER2

affibody and disulfide modification of DON displayed the strongest fluorescence compared to other groups, indicating their synergistic effect. To rule out the possibility that only disulfide-modified strands got internalized but not the DNA origami, four of the origami's staple strands were labeled with another fluorophore, Alexa Fluor 647 (Figure 3b). In agreement with the FAM-labeled DNA origami, a similar trend was observed in the Alexa Fluor 647-labeled DNA origami, with CytoDirect also demonstrating significantly higher cellular uptake efficiency.

Additionally, to further illustrate the influence of the disulfide distribution on DON, given that the hydrophobic effect of disulfide modification can influence the morphology of the structure, we designed three different distributions of disulfide modifications (termed the "even," "central," or "peripheral" distributions) on the DON and tested their difference in cellular uptake using flow cytometry (Figure S28). Both the central and evenly distributed disulfide modifications showed comparable efficiency in cellular uptake, whereas the peripheral distribution demonstrated a decreased cellular uptake efficacy. The reason for the decreased cellular uptake in the peripheral distribution might be due to increased aggregation formation. This is because the modification of disulfides on the peripheral side increases the likelihood of aggregate formation, which, in turn, hinders cellular uptake. CytoDirect was designed based on the central distribution of disulfide units.

To further investigate the impact of structural change on cellular uptake efficiency, induced by the hydrophobic-driven transition from planar to tubular structures following disulfide modification, we designed a HAF-DON tube. This tube was constructed using eight pairs of locking DNA strands to form a tubular configuration of HAF-DON that is similar to the tubular geometry of CytoDirect (Figure S29a). The formation of the HAF-DON tube was characterized by TEM, and the yield of HAF-DON tube monomers was approximately 80% (Figure S29b,c). We then assessed the cellular uptake of HAF-DON tube, HAF-DON sheet, and CytoDirect using CLSM and flow cytometry. The CLSM images showed that both the tubular and planar HAF-DON bound to the cell membrane of targeted cells, with the tubular HAF-DON exhibiting stronger fluorescence on the cell membrane compared to the HAF-DON sheet (Figure S30a). This suggests that tubular morphology may enhance the interaction of HAF-DON with the cell membrane. In contrast, CytoDirect displayed a significantly brighter and more uniform intracellular fluorescence distribution than both HAF-DON forms, which was evidenced by a significantly higher fluorescence intensity, as measured by flow cytometry, confirming the CLSM findings (Figure S30b). These findings suggest that the enhanced cytosolic uptake is primarily due to the synergistic effects of disulfide modification and HER2 affibody modification. The structural transition from planar to tubular also appears to amplify CytoDirect's binding to the cell membrane, potentially accelerating the disulfide exchange reaction and thereby enhancing cytosolic uptake. In summary, these results suggest that the disulfide modifications and HER2 affibodies synergistically enhance cytosolic uptake, with the improved cellular uptake attributed to the target-induced accelerated disulfide exchange reaction. Based on CLSM observations, we propose a possible four-stage sequence during the internalization of CytoDirect's uptake into SK-BR-3 cells, as illustrated in the schematic model (Figure 3c). Stage I: binding with the surface membrane by targeting the HER2 protein; Stage II:

proximity-induced efficient disulfide exchange; Stage III: direct translocation of CytoDirect to the cytoplasm; and Stage IV: GSH-assisted nanocarrier release from the cell membrane.

Cellular Distribution of CytoDirect.

Next, we analyzed the cellular distributions of CytoDirect, HAF-DON, and DS-DON by CLSM. SK-BR-3 cells were stained with LysoTracker to visualize the colocalization of DNA origami with late endosomes and lysosomes. As depicted in Figure 4, the green, fluorescent color was diffusely distributed within CytoDirect-treated cells, with only a few punctate bright spots colocalized with red-labeled late endosome or lysosomes. This distribution suggests that the cellular uptake of CytoDirect occurred primarily through an endocytosis-independent pathway. By contrast, without disulfide modification, HAF-DON was scarcely internalized inside the cells but instead remained on the cell membrane due to the binding with cell surface HER2 proteins. DON structures lacking a targeting module and disulfide modification were seldom taken up by the cells. Additionally, the Pearson's correlation coefficient of CytoDirect colocalization with late endosome and lysosomes was below 0.1 in SK-BR-3 cell (Figure S31). The subcellular distribution was also studied with a pH-insensitive fluorophore, Alexa Fluor 488 (Figure S32). More bright spots were observed colocalized with the LysoTracker signal than the FAM-labeled CytoDirect, which might indicate entrapment in the late endosome/lysosome. However, we consistently observed a strong green fluorescence signal with a diffuse distribution inside the cells when exposed to CytoDirect, compared to other groups. This observation strongly supports the direct cytosolic uptake of CytoDirect. It has been reported that there is a competition between direct translation and endocytosis of disulfides in thiol-mediated pathway, depending on the length and hydrophobicity of the disulfide units.[36] And the entrapment of CytoDirect is one possible reason why CytoDirect had a good tumor penetration effect (vide infra) since it requires both direct translation and endocytosis. Taken together, these findings indicated that CytoDirect can be efficiently internalized inside the cell via a predominantly endocytosis-independent pathway. We also evaluated the colocalization of disulfide-modified DON with late endosomes and lysosomes in HeLa cells (Figure S33). In comparison to 0SS-DON, 6SS-DON exhibited higher cellular uptake and did not colocalize with late endosomes or lysosomes, supporting the endocytosis-independent internalization. However, most of the green fluorescence signal still behaved as punctate spots, which implies sequestration in vesicle and aggregate formation. This result further highlights the importance of the targeting module for the cytosolic uptake of DNA nanostructures.

The observed variability in fluorescence distribution within the same treatment group can be primarily attributed to two main factors: (1) variability in the interaction of cell membrane with disulfide moieties on CytoDirect, influenced by inconsistent exposure (Figure S23) and possible degradation of disulfide units (Figure S24b,c), and (2) the influence of the cell cycle phase on cellular uptake,[37] with cells in the G2/M phase showing the highest efficiency, followed by S and G0/G1 phases, which might also impact the expression of membrane proteins crucial for the nanoparticle uptake.

Studying the Internalization Mechanism of CytoDirect.

To explore the mechanism underlying the highly efficient cellular uptake of CytoDirect, we pretreated SK-BR-3 cells with different cellular uptake inhibitors and studied the internalization of Alexa Fluor 488 labeled CytoDirect by CLSM and flow cytometry. These included sodium iodoacetate (a cell surface thiol inhibitor), chlorpromazine (CPZ, a clathrin-mediated endocytosis inhibitor), methyl-β-cyclodextrin (MβCD, a lipid raft inhibitor), and nystatin (NYS, a caveolin-mediated endocytosis inhibitor).[38–41] The cytotoxicities of different inhibitors were tested with a CCK-8 assay, and no obvious cytotoxicity was observed for all inhibitors (Figure S34). Previous studies have reported that DNA nanostructures are predominantly delivered into cells through clathrin- and caveolin-mediated endocytic pathways.[20] Our inhibition experiments indicated that CytoDirect undergoes thiol-mediated internalization in SK-BR-3 cells, as evidenced by the nearly complete inhibition of cellular uptake following the treatment of the cells with sodium iodoacetate. By contrast, the blockade of other pathways (i.e., caveolin, clathrin, and lipid raft) did not noticeably alter cellular uptake (Figure 5).

Tumor Penetration of CytoDirect in a 3D Multicellular Spheroid.

We next considered the tumor penetration ability of CytoDirect in deep tissue as this property is a crucial indicator for the evaluation of drug delivery systems. Multicellular spheroids have emerged as an attractive model for studying the penetration effect of nanoparticles across deep tissues, and such spheroids have also been applied to study the tumor penetration ability of DNA nanostructures.[42] Therefore, in this study, we compared the tumor penetration ability of CytoDirect versus that of HAF-DON in SK-BR-3 tumor spheroids in vitro. We prepared spheroids of SK-BR-3 cells with an average size of approximately 400 μm and incubated SK-BR-3 spheroids with 10 nM CytoDirect and HAF-DON for 4, 8, and 12 h, respectively (Figure 6a,b). The tumor penetration ability was tracked by 3D confocal microscopy. The 3D projection of fluorescence scanning revealed a distinct distribution pattern between CytoDirect and HAF-DON. Specifically, the distribution of FAM signals derived from CytoDirect demonstrated gradual penetration toward the central region of the tumor spheroid over time and was predominately localized to the central region after 12h incubation. In contrast, FAM from HAF-DON was modest, confined to the marginal areas of the spheroid, and decreased after 12 h. Collectively, these results underscore the excellent tumor penetration ability of CytoDirect.

Therapeutic Oligonucleotide and Small-Molecule Anticancer Drug Delivery by CytoDirect.

To assess the intracellular drug delivery efficiency of CytoDirect, we delivered two types of drug modalities (Figure 7a): the therapeutic oligonucleotide MCl-1 shRNA and the small-molecule chemotherapy drug doxorubicin. A tandem MCl-1 shRNA was designed to further increase the gene knockdown effectiveness of the shRNA, with its efficacy evaluated in HeLa and SK-BR-3 cells transfected with lipofectamine (Figure S35). MCl-1 shRNA was then delivered by CytoDirect through DNA-RNA hybridization. We investigated the gene knockdown effect of delivered MCl-1 shRNA in SK-BR-3 cells using a Western blot assay. Following a 24 h incubation period with different treatment methods, the MCl-1 shRNA delivered by CytoDirect outperformed all other groups in achieving the strongest gene

knockdown effect (~85%) (Figure 7b). Notably, the extent of protein inhibition mediated by shRNA delivered by CytoDirect surpassed that achieved with Lipofectamine (~70%), indicating the excellent functional payload delivery efficacy of CytoDirect. By contrast, shRNA delivered by the unmodified DON, or the disulfide-modified DON showed only a weak gene knockdown effect (~20% and ~30%, respectively). Meanwhile, shRNA delivered by a HER2 affibody-modified DNA origami showed a negligible gene silencing effect. This suggests that the tight binding of the HER2 affibody to the cell membrane HER2 protein might prolong the cell surface retention time and lead to the degradation of loaded shRNA, consistent with a previous report.[43] These results highlight the efficient delivery of MCl-1 shRNA by CytoDirect to the target SK-BR-3 cells.

After the successful delivery of shRNA, we explored the possibility of efficiently delivering small-molecule chemotherapy drugs to targeted cancer cells. Doxorubicin was loaded onto CytoDirect according to a previous report.[44] We determined the amount of doxorubicin intercalation into CytoDirect by measuring the absorption at 487 nm based on a doxorubicin standard curve (Figure S36). With this method, we calculated that each CytoDirect contains around 1850 doxorubicin molecules. We then compared the apoptosis induced by free doxorubicin and doxorubicin loaded onto CytoDirect in the SK-BR-3 cell line (Figure 7c). A propidium iodide (PI) and FITC-Annexin V co-staining assay was used to evaluate the cell conditions (viable, apoptotic, or necrotic). Compared to cells treated with free doxorubicin, confocal microscopy images of SK-BR-3 cells treated with the CytoDirect-delivered doxorubicin displayed a clear halo on the apoptotic membranes labeled with FITC-Annexin V. Meanwhile, PI also efficiently labeled the nuclei of these cells, indicating damage to membrane integrity. However, cells treated with free doxorubicin largely maintained a well-stretched morphology, indicating a healthy condition. Taken together, these results suggest that CytoDirect can deliver doxorubicin to targeted cancer cells with greater efficiency than free doxorubicin and effectively initiate the apoptotic process in these cells.

CONCLUSIONS

In summary, we demonstrated that the synergistic effect of disulfide and HER2 affibody modifications on the DNA origami template results in rapid cytosolic uptake and excellent tumor penetration ability for targeted drug delivery, leading to high levels of therapeutic efficacy. By leveraging experience from the field of DNA nanotechnology, we modified the unique properties of disulfide units and HER2 affibody onto a biocompatible and programmable DNA origami template for cytosolic delivery to targeted cells. The disulfide-modified DON displayed a tubular shape due to the hydrophobic effect of the disulfide protection groups, and this tubular shape prevented the aggregation of the hydrophobic disulfide patches. We also highlight that the DNA origami nanostructures enabled an extremely high density of disulfides (104 copies of 6-repeat disulfides per structure) in order to further enhance uptake of the highly anionic nanostructure. HER2 affibody modification endowed the DNA nanocarrier with target specificity to HER2-overexpressing breast cancer cells, leading to the adjacence of disulfide units and cell surface thiol groups, followed by an accelerated disulfide exchange reaction. DNA origami modified with both disulfide units and the HER2 affibody demonstrated significantly higher cellular uptake efficiency than with a single module modification or without any modifications. The distinct stages of

internalization were observed from a time-course study, although the precise entry process is still under investigation. It is noteworthy that CytoDirect exhibited a diffuse distribution inside the cytoplasm, which addresses the challenging problem of using DNA origami as a drug delivery platform. Access to deep tissue has always been challenging as it requires a balance between transcytosis and cytosolic release. An excellent tumor penetration capacity was found for our designed CytoDirect, and the mechanistic study further supports the predominately thiol-mediated direct translocation.

This work demonstrates a unique drug delivery system that can deliver both oligonucleotide and small-molecule drugs rapidly and directly to the cytoplasm of targeted cells and deep tissue. Future studies will improve our understanding of the uptake process and membrane trafficking pathways at the single particle level as well as evaluate their biodistribution, efficacy, and biosafety in vivo. This study expands the usage of DNA nanostructures as a delivery system and demonstrates the translational potential of DNA nanostructure-based nanocarriers.

Supplementary Material

Refer to Web version on PubMed Central for supplementary material.

ACKNOWLEDGMENTS

This work was supported by Arizona State University, and N.S. acknowledges support from NIH under grant number DP2GM132931. The content is solely the responsibility of the authors and does not necessarily represent the official views of the National Institutes of Health.

REFERENCES

(1). Kim BY; Rutka JT; Chan WC Nanomedicine. N. Engl. J. Med 2010, 363 (25), 2434–2443. [PubMed: 21158659]

(2). Roberts TC; Langer R; Wood MJA Advances in oligonucleotide drug delivery. Nat. Rev. Drug Discovery 2020, 19 (10), 673–694. [PubMed: 32782413]

(3). Zhang Y; Hu Y; Tian H; Chen X Opportunities and Challenges for mRNA Delivery Nanoplatforms. J. Phys. Chem. Lett 2022, 13 (5), 1314–1322. [PubMed: 35107010]

(4). Vargason AM; Anselmo AC; Mitragotri S The evolution of commercial drug delivery technologies. Nat. Biomed. Eng 2021, 5 (9), 951–967. [PubMed: 33795852]

(5). Kretzmann JA; Liedl A; Monferrer A; Mykhailiuk V; Beerkens S; Dietz H Gene-encoding DNA origami for mammalian cell expression. Nat. Commun 2023, 14 (1), No. 1017, DOI: 10.1038/s41467-023-36601-1.

(6). Jiang Q; Song C; Nangreave J; Liu X; Lin L; Qiu D; Wang Z-G; Zou G; Liang X; Yan H; Ding B DNA Origami as a Carrier for Circumvention of Drug Resistance. J. Am. Chem. Soc 2012, 134 (32), 13396—13403. [PubMed: 22803823]

(7). Ikwuagwu B; Tullman-Ercek D Virus-like particles for drug delivery: a review of methods and applications. Curr. Opin Biotechnol 2022, 78, No. 102785.

(8). Tam YY; Chen S; Cullis PR Advances in Lipid Nanoparticles for siRNA Delivery. Pharmaceutics 2013, 5 (3), 498–507. [PubMed: 24300520]

(9). Tai W; Zhao P; Gao X Cytosolic delivery of proteins by cholesterol tagging. Sci. Adv 2020, 6 (25), No. eabb0310, DOI: 10.1126/sciadv.abb0310.

(10). Sun Y; Lau SY; Lim ZW; Chang SC; Ghadessy F; Partridge A; Miserez A Phase-separating peptides for direct cytosolic delivery and redox-activated release of macromolecular therapeutics. Nat. Chem 2022, 14 (3), 274–283. [PubMed: 35115657]

(11). Pu X; Li J; Qiao P; Li M; Wang H; Zong L; Yuan Q; Duan S Mesoporous Silica Nanoparticles as a Prospective and Promising Approach for Drug Delivery and Biomedical Applications. Curr. Cancer Drug Targets 2019, 19 (4), 285–295. [PubMed: 30520373]

(12). Shokri E; Hosseini M; Davari MD; Ganjali MR; Peppelenbosch MP; Rezaee F Disulfide-induced self-assembled targets: A novel strategy for the label free colorimetric detection of DNAs/RNAs via unmodified gold nanoparticles. Sci. Rep 2017, 7, No. 45837, DOI: 10.1038/srep45837.

(13). Dey S; Fan C; Gothelf KV; Li J; Lin C; Liu L; Liu N; Nijenhuis MAD; Saccà B; Simmel FC; Yan H; Zhan P DNA origami. Nat. Rev. Methods Primers 2021, 1, 13 DOI: 10.1038/s43586-020-00009-8.

(14). Woo S; Rothemund PW Programmable molecular recognition based on the geometry of DNA nanostructures. Nat. Chem 2011, 3 (8), 620–627. [PubMed: 21778982]

(15). Seeman NC; Sleiman HF DNA Nanotechnology. Nat. Rev 2017, 3, No. 17068, DOI: 10.1038/natrevmats.2017.68.

(16). Zhang F; Nangreave J; Liu Y; Yan H Structural DNA nanotechnology: state of the art and future perspective. J. Am. Chem. Soc 2014, 136 (32), 11198–11211. [PubMed: 25029570]

(17). Jiang S; Ge Z; Mou S; Yan H; Fan C Designer DNA nanostructures for therapeutics. Chem 2021, 7 (5), 1156–1179.

(18). Madhanagopal BR; Zhang S; Demirel E; Wady H; Chandrasekaran AR DNA Nanocarriers: Programmed to Deliver. Trends Biochem. Sci 2018, 43 (12), 997–1013. [PubMed: 30342801]

(19). Jiang Q; Liu S; Liu J; Wang ZG; Ding B Rationally Designed DNA-Origami Nanomaterials for Drug Delivery In Vivo. Adv. Mater 2019, 31 (45), No. e1804785, DOI: 10.1002/adma.201804785.

(20). Wang P; Rahman MA; Zhao Z; Weiss K; Zhang C; Chen Z; Hurwitz SJ; Chen ZG; Shin DM; Ke Y Visualization of the Cellular Uptake and Trafficking of DNA Origami Nanostructures in Cancer Cells. J. Am. Chem. Soc 2018, 140 (7), 2478–2484. [PubMed: 29406750]

(21). Gasparini G; Bang EK; Montenegro J; Matile S Cellular uptake: lessons from supramolecular organic chemistry. Chem. Commun 2015, 51 (52), 10389–10402.

(22). Torres AG; Gait MJ Exploiting cell surface thiols to enhance cellular uptake. Trends Biotechnol. 2012, 30 (4), 185–190. [PubMed: 22260747]

(23). Shu Z; Tanaka I; Ota A; Fushihara D; Abe N; Kawaguchi S; Nakamoto K; Tomoike F; Tada S; Ito Y; Kimura Y; Abe H Disulfide-Unit Conjugation Enables Ultrafast Cytosolic Internalization of Antisense DNA and siRNA. Angew. Chem., Int. Ed 2019, 58 (20), 6611–6615.

(24). Zhou J; Sun L; Wang L; Liu Y; Li J; Li J; Li J; Yang H Self-Assembled and Size-Controllable Oligonucleotide Nanospheres for Effective Antisense Gene Delivery through an Endocytosis-Independent Pathway. Angew. Chem., Int. Ed 2019, 58 (16), 5236–5240.

(25). Oh DY; Bang YJ HER2-targeted therapies - a role beyond breast cancer. Nat. Rev. Clin. Oncol 2020, 17 (1), 33–48. [PubMed: 31548601]

(26). Swain SM; Shastry M; Hamilton E Targeting HER2-positive breast cancer: advances and future directions. Nat. Rev. Drug Discovery 2023, 22 (2), 101–126. [PubMed: 36344672]

(27). Eigenbrot C; Ultsch M; Dubnovitsky A; Abrahmsen L; Hard T Structural basis for high-affinity HER2 receptor binding by an engineered protein. Proc. Natl. Acad. Sci. U.S.A 2010, 107 (34), 15039–15044. [PubMed: 20696930]

(28). Ambrosetti E; Bernardinelli G; Hoffecker I; Hartmanis L; Kiriako G; de Marco A; Sandberg R; Högberg B; Teixeira AI A DNA-nanoassembly-based approach to map membrane protein nanoenvironments. Nat. Nanotechnol 2021, 16 (1), 85–95. [PubMed: 33139936]

(29). Zhang C; Han M; Zhang F; Yang X; Du J; Zhang H; Li W; Chen S Enhancing Antitumor Efficacy of Nucleoside Analog 5-Fluorodeoxyuridine on HER2-Overexpressing Breast Cancer by Affibody-Engineered DNA Nanoparticle. Int. J. Nanomed 2020, 15, 885–900.

(30). Sample M; Liu H; Matthies M; Šulc P Hairygami: Analysis of DNA Nanostructure's Conformational Change Driven by Functionalizable Overhangs arXiv preprint, Submitted: 2023–02–17, 2023. DOI: 10.48550/arXiv.2302.09109 (accessed November 08, 2023).

(31). Snodin BEK; Randisi F; Mosayebi M; Šulc P; Schreck JS ; Romano F; Ouldridge TE; Tsukanov R; Nir E; Louis AA; Doye JPK Introducing improved structural properties and salt dependence

into a coarse-grained model of DNA. J. Chem. Phys 2015, 142 (23), No. 234901, DOI: 10.1063/1.4921957.

(32). Hu YB; Dammer EB; Ren RJ; Wang G The endosomal-lysosomal system: from acidification and cargo sorting to neurodegeneration. Transl. Neurodegener 2015, 4, No. 18, DOI: 10.1186/s40035-015-0041-1.

(33). Lorenz S; Tomcin S; Mailander V Staining of mitochondria with Cy5-labeled oligonucleotides for long-term microscopy studies. Microsc. Microanal 2011, 17 (3), 440–445. [PubMed: 21600074]

(34). Lacroix A; Vengut-Climent E; de Rochambeau D; Sleiman HF Uptake and Fate of Fluorescently Labeled DNA Nanostructures in Cellular Environments: A Cautionary Tale. ACS Cent. Sci 2019, 5 (5), 882–891. [PubMed: 31139724]

(35). Yang W; Liu X; Li H; Zhou J; Chen S; Wang P; Li J; Yang H Disulfide-Containing Molecular Sticker Assists Cellular Delivery of DNA Nanoassemblies by Bypassing Endocytosis. CCS Chem. 2021, 3 (3), 1178–1186.

(36). Martinent R; Tawffik S; Lopez-Andarias J; Moreau D; Laurent Q; Matile S Dithiolane quartets: thiol-mediated uptake enables cytosolic delivery in deep tissue. Chem. Sci 2021, 12 (41), 13922–13929. [PubMed: 34760179]

(37). Kim JA; Aberg C; Salvati A; Dawson KA Role of cell cycle on the cellular uptake and dilution of nanoparticles in a cell population. Nat. Nanotechnol 2012, 7 (1), 62–68.

(38). Kanjilal P; Dutta K; Thayumanavan S Thiol-Disulfide Exchange as a Route for Endosomal Escape of Polymeric Nanoparticles. Angew. Chem., Int. Ed 2022, 61 (37), No. e202209227, DOI: 10.1002/anie.202209227.

(39). Ng CT; Tang FM; Li JJ; Ong C; Yung LL; Bay BH Clathrin-mediated endocytosis of gold nanoparticles in vitro. Anat. Rec 2015, 298 (2), 418–427.

(40). Mahammad S; Parmryd I Cholesterol depletion using methyl-beta-cyclodextrin. Methods Mol. Biol 2015, 1232, 91–102. [PubMed: 25331130]

(41). Plummer EM; Manchester M Endocytic uptake pathways utilized by CPMV nanoparticles. Mol. Pharmaceutics 2013, 10 (1), 26–32.

(42). Wang Y; Benson E; Fordos F; Lolaico M; Baars I; Fang T; Teixeira AI; Hogberg B DNA Origami Penetration in Cell Spheroid Tissue Models is Enhanced by Wireframe Design. Adv. Mater 2021, 33 (29), No. e2008457, DOI: 10.1002/adma.202008457.

(43). Shi Q; Wu Y; Xu Y; Bao M; Chen X; Huang K; Yang Q; Yang Y Virus Mimetic Framework DNA as a Non-LNP Gene Carrier for Modulated Cell Endocytosis and Apoptosis. ACS Nano 2023, 17 (3), 2460–2471. [PubMed: 36693051]

(44). Wang Z; Song L; Liu Q; Tian R; Shang Y; Liu F; Liu S; Zhao S; Han Z; Sun J; Jiang Q; Ding B A Tubular DNA Nanodevice as a siRNA/Chemo-Drug Co-delivery Vehicle for Combined Cancer Therapy. Angew. Chem., Int. Ed 2021, 60 (5), 2594–2598.

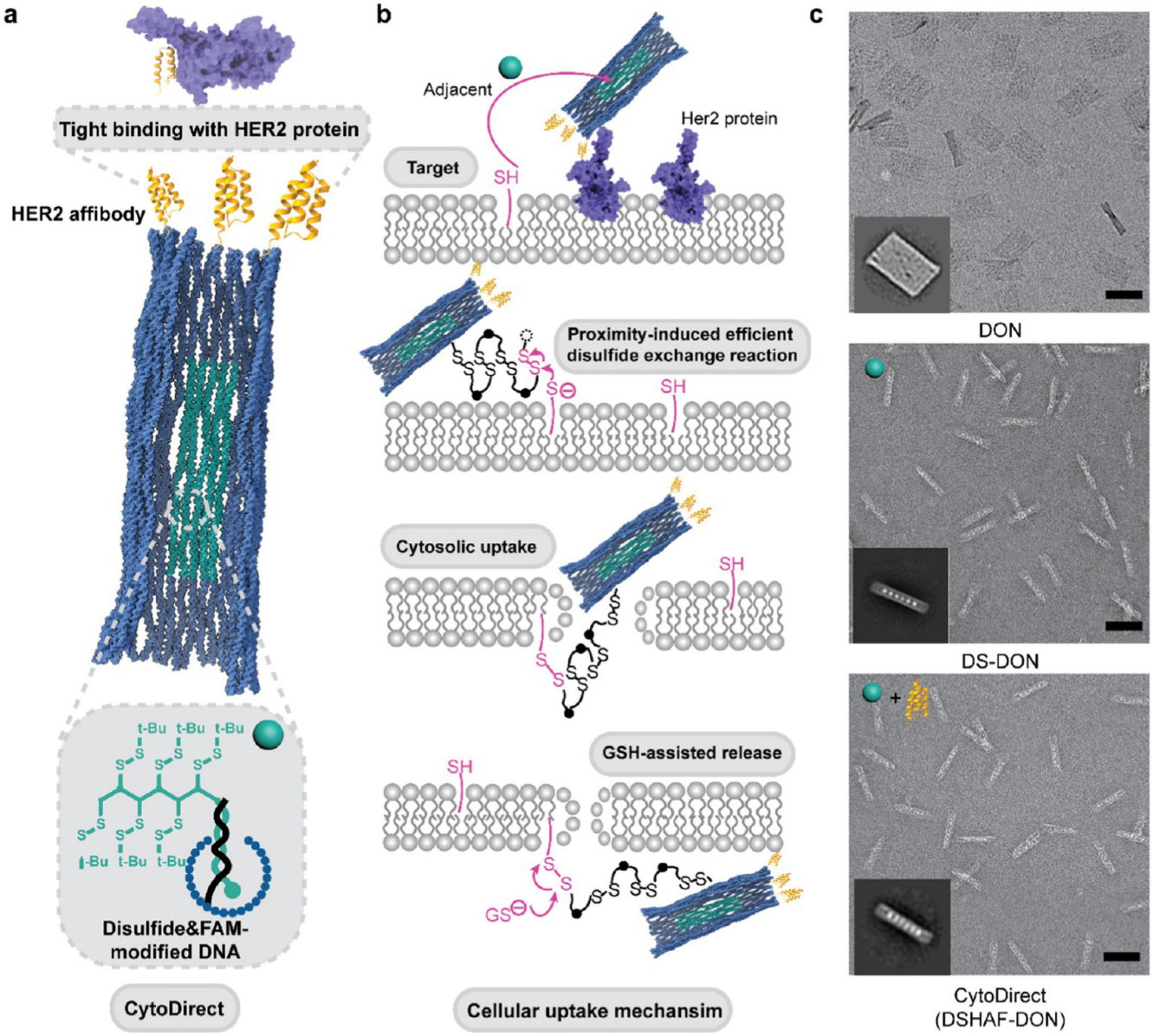

Figure 1.

Design and characterization of the CytoDirect DNA nanodevice. (a) Illustration of the construction of the disulfide- and HER2 affibody-modified CytoDirect. (b) Schematic illustration of the proximity-induced, thiol-mediated rapid cytosolic uptake process. (c) Representative negative stain TEM images of DON, DS-DON, and CytoDirect. Insets represent 2D class average images. Scale bar, 100 nm.

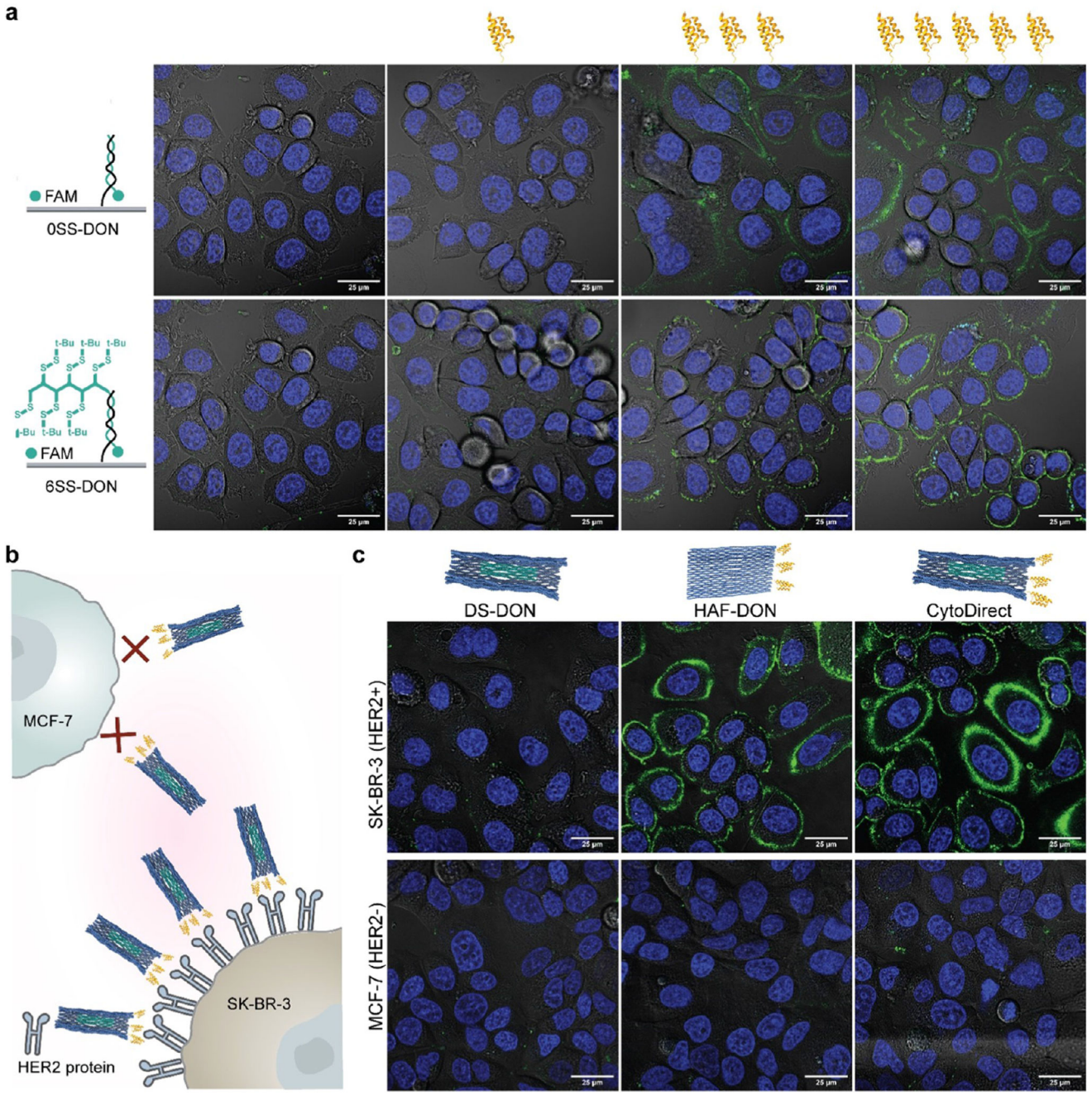

Figure 2.

Comparison of target specificity of FAM-labeled DS-DON, HAF-DON, and CytoDirect in HER2-positive and -negative breast cancer cells. (a) Targeting ability of HER2-modified FAM-labeled DON (3 nM) in relation to the number (0, 1, 3, and 5) of modified HER2 affibodies in cells overexpressing HER2. HER2-modified DONs were incubated with SK-BR-3 cells for 30 min. Scale bar, 25 μm. (b) Schematic illustration of the interaction between the HER2 protein, expressed on the membrane of SK-BR-3 cells, and the HER2 affibodies modified on DON (3 nM). (c) Representative confocal microscopy images of

SK-BR-3 (HER2-positive) and MCF-7 (HER2-negative) cells, following incubation with FAM-labeled 3 nM DS-DON, HAF-DON, and CytoDirect (green) for 30 min. Scale bar, 25 μm.

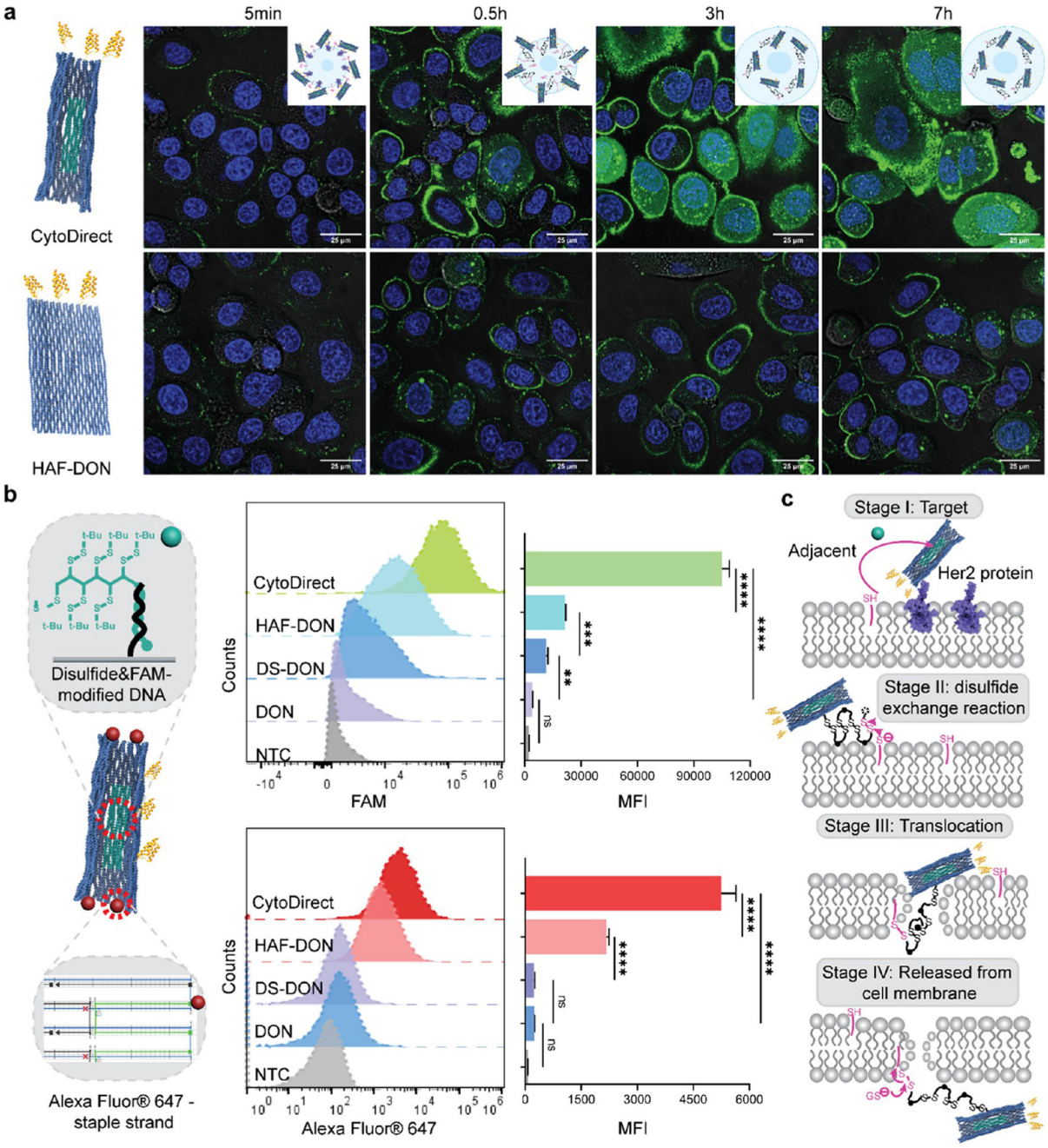

Figure 3.

Cellular uptake of DNA nanocarrier with different modifications. (a) Representative confocal microscopy images of HER2 affibody-modified FAM-labeled DNA nanocarrier with disulfide (top) and without disulfide (bottom) modification at different time points (5 min, 0.5 h, 3 h, and 7 h; scale bar, 25 μm). (b) Flow cytometry analysis of the internalization of both FAM and Alexa Fluor 647-labeled DNA nanocarrier (3 nM) with different modifications. FAM labeled with or without disulfide-modified hybridized strand (top). Alexa Fluor 647-labeled staple strands of DNA origami (bottom). Error bars represent

mean ± s.d. 0.1234 (ns), 0.0332 (*P), 0.0021 (**P), 0.0002 (***P), < 0.0001 (****P) from three independent experiments. **c.** Proposed four-stage internalization process of CytoDirect.

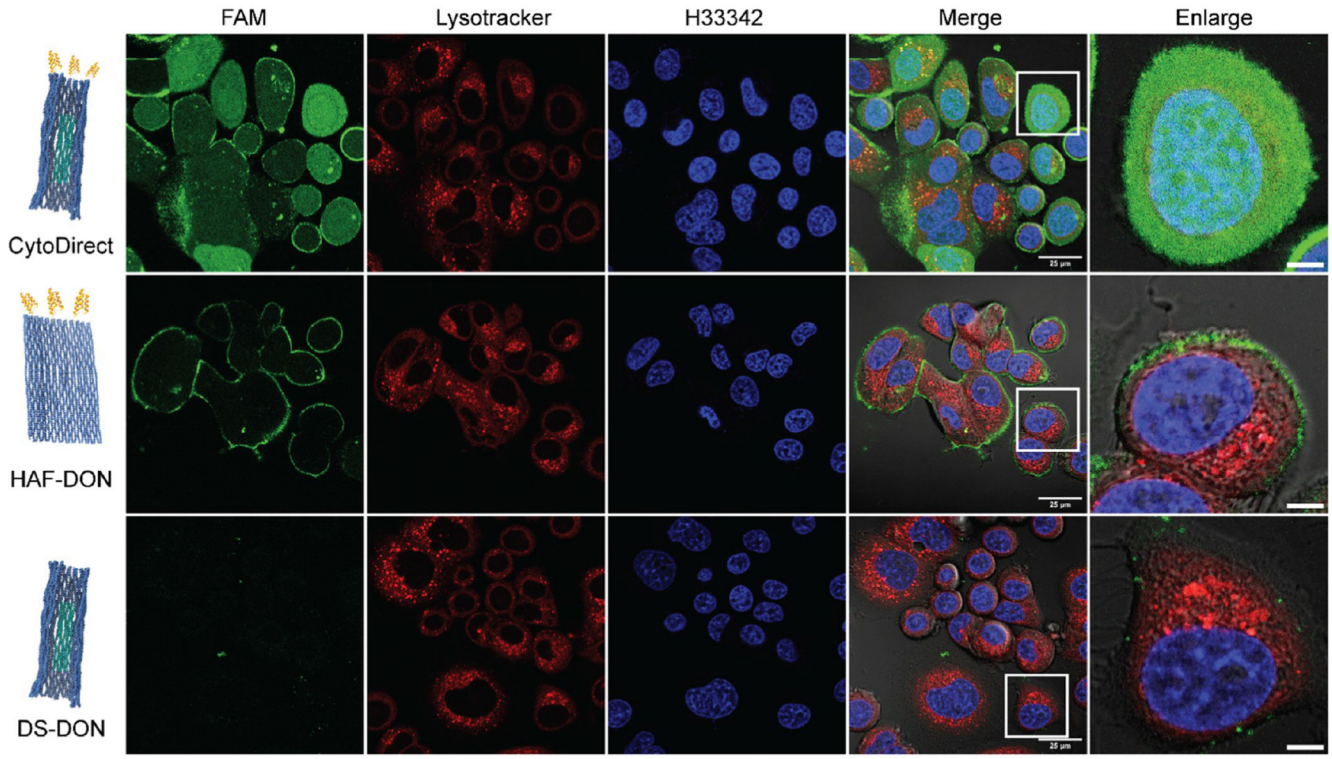

Figure 4.

Cell distribution of FAM-labeled DNA nanocarriers with different modifications. Confocal microscopy image of SK-BR-3 cells treated with 3 nM CytoDirect, HAF-DON, and DS-DON (green) for 5 h. The nucleus was stained with Hoechst 33342 (blue), and the late endosome and lysosome were stained with LysoTracker (red). Scale bar: 25 μm. Enlarged images are the amplified images of the white boxed regions in the merged channels. Scale bar, 5 μm. CytoDirects were diffused in the cytoplasm of cells.

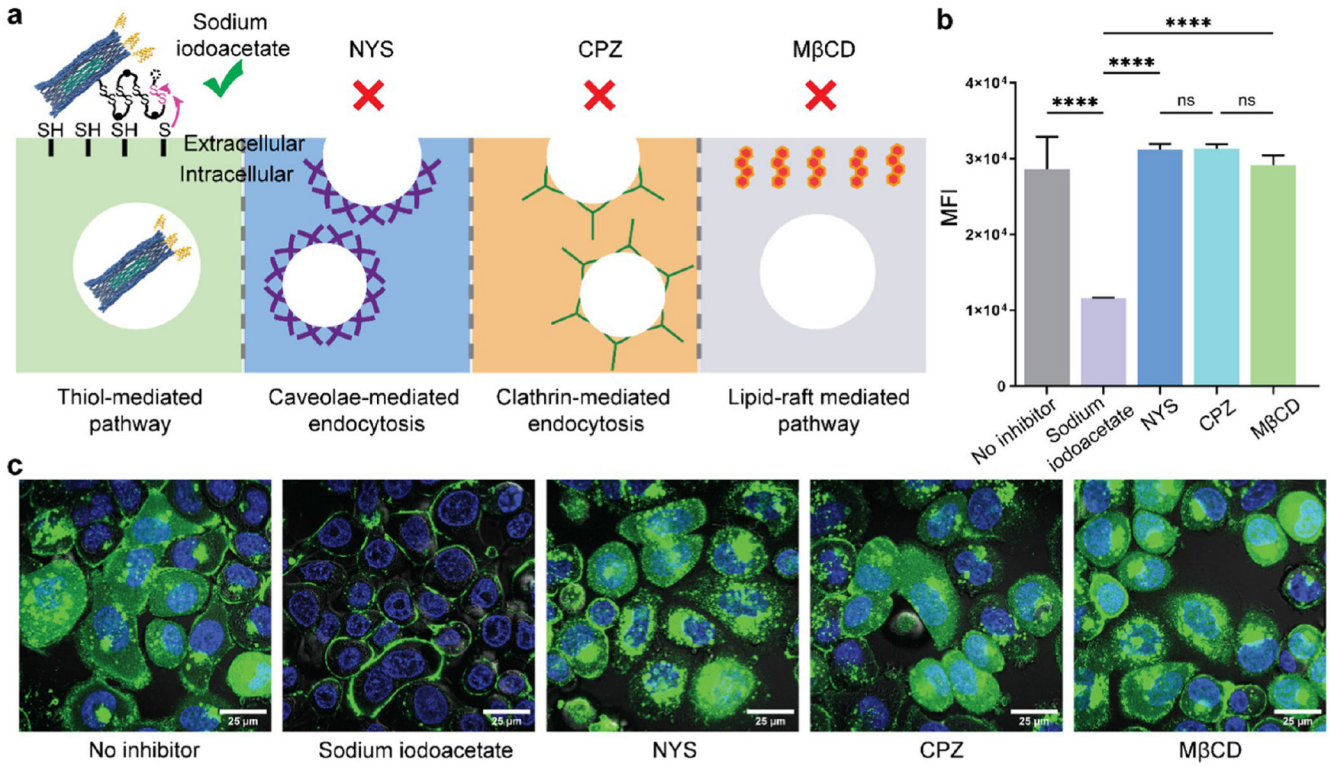

Figure 5.

Inhibitory assays to probe cellular uptake mechanism of Alexa Fluor 488 labeled CytoDirect. (a) Schematic summary of the cellular uptake mechanisms of thiol-mediated pathway and endocytic pathways. (b, c) Flow cytometry and CLSM results of the cellular uptake of 3 nM Alexa Fluor 488 labeled CytoDirect in SKBR3 cells with pretreatment of different inhibitors, including 1.2 mM sodium iodoacetate, 2.5 μg/100 μL nystatin (NYS), 10 μM chloropromazine (CPZ), and3 mM methyl-β-cyclodextrin. Scale bar: 25 μm.

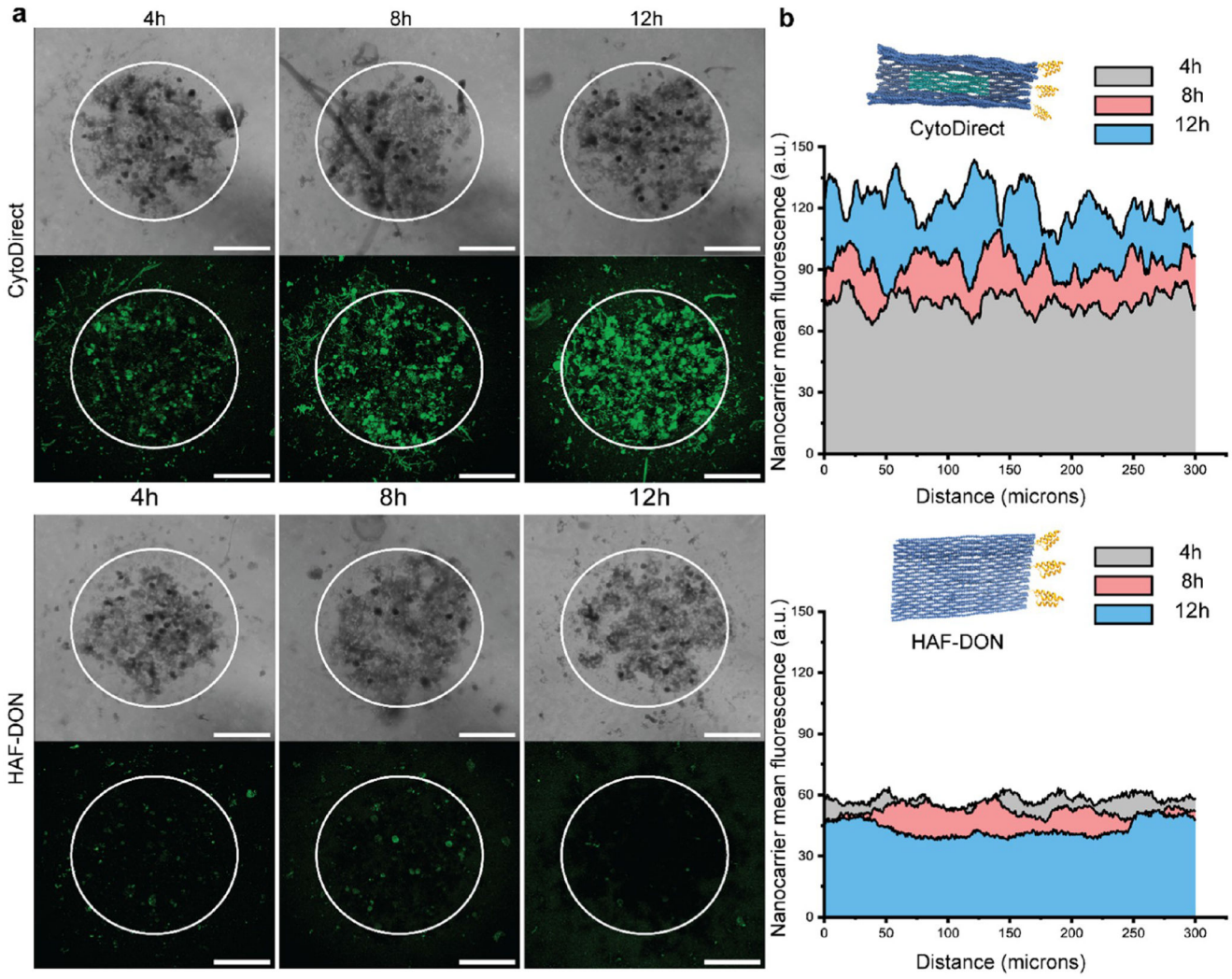

Figure 6.

Tumor penetration study of FAM-labeled CytoDirect and HAF-DON. (a) 3D projection images of SK-BR-3 spheroids incubated with 10 nM CytoDirect and HAF-DON for 4, 8, and 12 h, respectively. Scale bar, 200 μm. (b) Radial distribution plots of CytoDirect and HAF-DON in a 3D SK-BR-3 tumor spheroid.

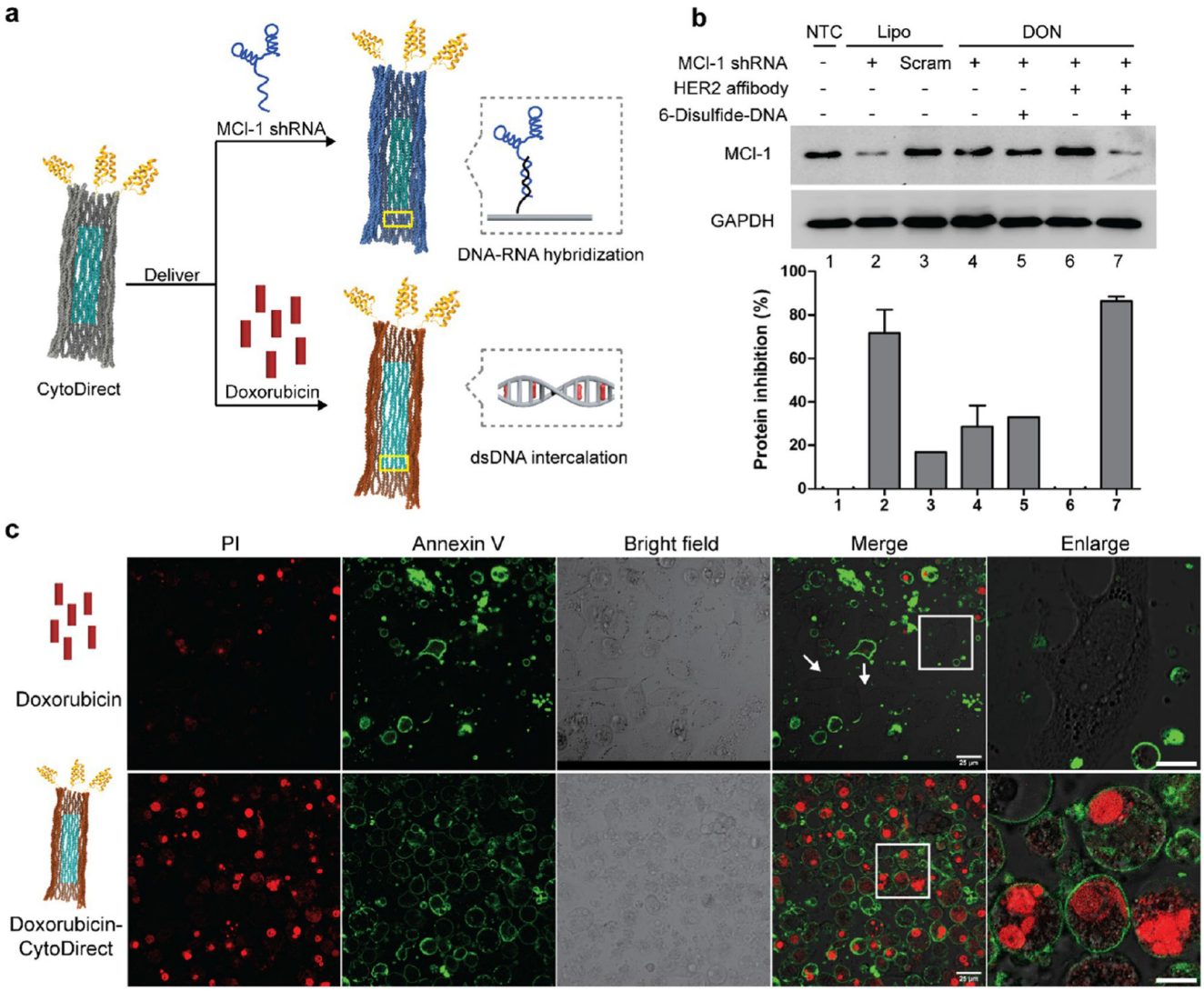

Figure 7.

CytoDirect delivery of MCl-1 shRNA and the anticancer drug doxorubicin to SK-BR-3 cells. (a) Schematic illustration of using the CytoDirect to deliver MCl-1 shRNA by DNA-RNA hybridization and delivering doxorubicin by intercalation into double-stranded DNA. (b) Gene knockdown effect of CytoDirect-delivered MCl-1 shRNA determined by Western blot. (c) Comparison of SK-BR-3 cell apoptosis between free doxorubicin and CytoDirect-delivered doxorubicin by FITC-Annexin V (green) and PI (red) co-staining. Scale bar, 25 μm. White arrows in the upper merged channel represent viable cells. Enlarged images are amplified images of the white boxed regions in the merged channels. Scale bar, 10 μm.